Measuring hydraulic layer resistance and correlated effects in colloidal fouling of salt-retaining membranes

M. Keller, S. Panglisch and R. Gimbel

ABSTRACT

Colloidal fouling is one of the main reasons for the reduced efficiency of membrane-based water desalination processes. The synchrony of several resistance mechanisms like hydraulic, osmotic, and electro-kinetic as well as numerous coupling effects complicate the analysis of their individual contributions to the fouling extent. A new measuring approach using a dead-end filtration test-cell allows exactly this, irrespective of any simultaneously occurring concentration polarization phenomena. First results show that the hydraulic resistance of a fully developed colloidal layer is not exclusively determined by the physicochemical properties of its constituents but seems to be strongly dependent on the specific way of its formation (e.g. ionic strength prevailing during layer build-up or filtration sequence of different particle sizes). This time-dependent effect is largely irreversible and therefore most likely due to persistent changes in fouling layer structure. A minor reversible ionic strength effect could also be demonstrated. The extent of this effect is identical irrespective of whether the ionic strength is increased or decreased. Results further indicate that commonly applied models like the Kozeny–Carman equation are lacking a size-dependent parameter that causes a disproportionate decrease of colloidal fouling layer resistance with decreasing foulant particle size.

Key words | colloidal fouling, dead-end experiments, dense membranes, modelling, osmotic pressure

M. Keller (corresponding author)
S. Panglisch
R. Gimbel
University Duisburg-Essen (UDE), Chair of Mechanical Process Engineering/Water Technology,
Lotharstr. 1,
Duisburg 47057,
Germany
E-mail: *mathis.keller@uni-due.de*

INTRODUCTION

The deposition of water constituents on the membrane surface in solid or gel-like form (fouling) usually has the effect that a fluid passing the membrane at a constant rate experiences a higher pressure drop than in an equivalent case without fouling. This additional pressure loss significantly influences the total energetic efficiency of the filtration process and is attributed to molecular friction in the stationary fouling layer. This 'hydraulic' resistance is frequently referred to as a pure material parameter that is solely determined by the geometric properties of the substances that form the fouling layer. Since membrane desalination processes are usually applied to treat raw waters with low particulate loads, the relevant fouling substances are mostly in the colloidal size range. Nevertheless the models that are commonly applied to describe colloidal fouling layer resistance are usually based on concepts that have been developed for macroscopic (particulate) systems. Most of these models only work within the scope of the Darcy equation and incorporate the significant structural parameters of the respectively described layers. Among the most accepted and frequently applied semi-empirical models for the description of densely packed particle layers are the models of Brinkman, Rumpf and Gupte, as well as the well-known model of Kozeny and Carman (Dullien 1992). For suspended layers and macromolecular gels that lack a defined pore structure mostly cell models like

doi: 10.2166/ws.2016.181

that of Happel or Kuwabara are applied (Masliyah & Bhattacharjee 2006).

The attempt to analytically verify the applicability of such models for the colloidal size range has often failed due to the limitations of the available in-situ visualization techniques. Due to this, the structural properties of colloidal layers, as they usually form under practically relevant operating conditions on desalination membranes, have never been systematically specified in a representative and reliable way. On the other hand, a quantitative evaluation of the predictive accuracy of these resistance models is challenging even under well-controlled laboratory conditions, as the measured increase in transmembrane pressure (TMP), mostly taken as an indicator for changes in the hydraulic resistance, is actually a kind of sum parameter that quantifies the effectiveness of various resistance mechanisms simultaneously.

Besides the 'hydraulic' resistance mechanisms, which are related to molecular friction effects, the TMP increase in membrane-based desalting applications is most significantly affected by osmotic and electro-kinetic mechanisms (Michaels & Lin 1955; Nirschl & Schäfer 2005), which are related to the ion retention of the applied membrane material. Moreover, caused by the much greater importance of molecular interactions in colloidal fouling layers the structural properties predominantly determining their overall resistance are stronger depending on the applied operational settings and the raw water composition as in particulate fouling layers (Tang *et al.* 2011; Sim *et al.* 2014). A colloidal layer structure is particularly susceptible to changes in raw water ionic strength strongly affecting the electrostatic repulsion between like-charged particles. In this context a deviation from the practically relevant filtration conditions for the purpose of a selective experimental analysis of individual resistance mechanisms has to be assessed critically.

The differentiation between individual contributions of superimposed resistance mechanisms is further complicated by the existence of coupling effects that relate the effectiveness of a resistance mechanism (as well as the extent of its contributed resistance) to the simultaneous occurrence and the effectiveness of another resistance mechanism. A prominent example of this kind of coupling effect is the cake enhanced osmotic pressure (CEOP) phenomenon (Hoek & Elimelech 2003; Sim *et al.* 2011), whereby the diffusibility of salt ions that are retained by the membrane is reduced by the predetermined tortuous pathways in the porous colloidal fouling layer (Shen & Chen 2007). The respectively increased ion concentration at the feed-side membrane surface leads to an increase in concentration polarization (CP) and consequently in transmembrane osmotic pressure. Nevertheless, in the presence of dense fouling layers, which possess salt-retaining properties by themselves, contrary effects were also observed (Kim *et al.* 2009). Other coupling effects are, for example, related to fouling-induced changes in the ion retentive characteristics or the water permeability of the applied membrane materials (Lipp *et al.* 1994; Mahlangu *et al.* 2014). Due to the practically difficult differentiation between resistance mechanisms and coupling effects the contribution of specific coupling effects to the overall resistance has rarely been described quantitatively. Depending on the considered raw water qualities and the specifically applied operating conditions the existing studies differ widely in the assessment of their relative importance.

The present study aimed to develop a new measuring procedure that enables the quantitative separation between different types of hydraulic layer resistances and correlations with their respective causes. Since the physicochemical circumstances that influence the formation of fouling and/or CP layers are often heterogeneous and difficult to control across the full filtration module length, this goal can hardly be achieved in cross-flow (CF) mode.

MATERIALS AND METHODS

The measuring procedure has been specifically developed in order to quantify individual resistances of typical fouling layer types. Due to the well controllable and highly reproducible physicochemical filtration conditions, a dead-end (DE) filtration method is chosen instead of more commonly applied CF filtration methods. Thereby, the limited practical relevance of the method in desalting applications is accepted in favor of the potentially significant lesser susceptibility against system-specific measuring artifacts. The direct comparison of DE and CF measuring methods, however, is beyond the scope of the present article and will be a topic of future publications. In order to evaluate the accuracy of

the method and allow for comparison of measuring results and predictions of geometry-based resistance models, only model foulants with ideal geometrical properties are applied.

Methodological considerations

When a membrane is operated in CF mode, CP is affected twofold. Firstly CF induced flow field instabilities within the feed flow channel limit the thickness of the CP-layer. According to film-layer theory this instance has a direct effect on the salt concentration gradient and the mass transfer in the layer. Secondly the total amount of salt within the membrane module and therewith the maximum extent of CP is restricted.

When a fouling layer is established at the membrane surface, which partially or fully superimposes the CP-layer, the hydrodynamic conditions that the CP-layer is exposed to change and CP as well as its related effect on TMP are affected to an unknown (highly situation-specific) extent. The implications of further influences that change the mass transfer within the CP-layer, e.g. CEOP, can hardly be distinguished from that effect. Therefore, with respect to the notations given in Figure 1(a), the fouling-related change in salt concentration $c_{s,m,a}$ on the membrane surface cannot be experimentally determined precisely without applying highly sensitive sensor technology equipment with extraordinary spatial resolution.

In DE mode the described CP-limiting effects do not apply. Therefore, when a salt solution is filtered at a constant volumetric membrane flux $\dot{J}_M$, $c_{s,m,a}$ will increase until either the solubility limit is reached and salt precipitates at the membrane surface or the molar salt transfer rate through the membrane $\dot{N}_{M,s}$ reaches an ultimate level at which the salt concentration in the bulk $c_{s,b}$ equals the concentration in the permeate $c_{s,p}$. The latter case, as depicted in Figure 1(b), is particularly realistic if nanofiltration (NF) or brackish water reverse osmosis (BW-RO) membranes with only partial salt retention are considered. For this specific steady-state situation the following three conditions apply:

$$(1)\ \frac{c_{s,p}}{c_{s,b}} = 1 \text{ and respectively } \Re_{M,s}^{app} = \frac{c_{s,b} - c_{s,p}}{c_{s,b}} = 0$$

$$(2)\ \frac{c_{s,m,a}}{c_{s,b}} = \max. \text{ and respectively}$$

$$\Re_{M,s}^{eff} = \frac{c_{s,m,a} - c_{s,p}}{c_{s,m,a}} = \max.$$

$$(3)\ \frac{\dot{N}_{M,s}}{\dot{N}_{M,w}} = \frac{c_{s,b}}{c_{w,b}} = \frac{c_{s,p}}{c_{w,p}} = \text{constant}$$

Herein $\Re_{M,s}^{app}$ and $\Re_{M,s}^{eff}$ are the apparent and the effective membrane retention, respectively. Assuming constant $\Re_{M,s}^{eff}$ the steady-state conditions given above are valid irrespective of any emerging membrane fouling since any further fouling-related deviation of $c_{s,m,a}$ (e.g. as proposed by the CEOP model) would, according to solution diffusion model, inevitably lead to an increase in $\dot{N}_{M,s}$. An increase in $\dot{N}_{M,s}$ however would generate the paradoxical situation that more salt ions are transported through the membrane than are contained in the feed water stream. Therefore, $c'_{s,m,a}$ (the index $'$ indicates steady-state condition) has to be

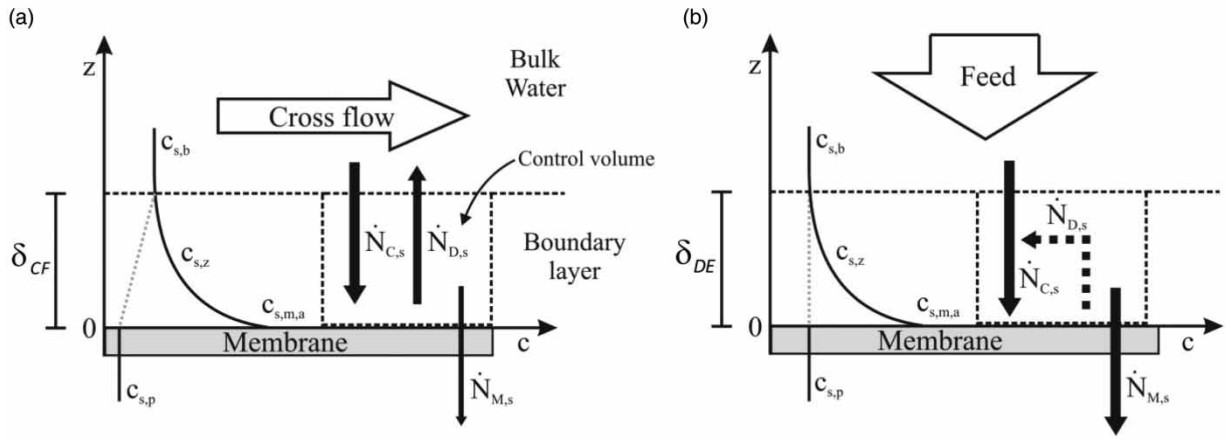

Figure 1 | Steady-state concentration polarization in (a) cross-flow and (b) dead-end mode operation.

considered as a limiting concentration for a given filtration situation that is independent of the applied (constant) water flux according to condition 3.

Filtration apparatus

Colloidal fouling experiments were performed using a cylindrical DE-filtration cell with an inner diameter of 34 mm and an active membrane area of 9.08 cm^2. The filtration cell is specifically laid out in order to produce a laminar flow with stream lines running parallel towards the membrane surface. The special injector through which the feed enters the filtration cell has openings rectangular to the main flow direction within the filtration cell and therewith ensures a uniform horizontal distribution of the foulant particles across the establishing flow profile. The filtration cell is contained in a double-walled metal jacket, which is connected to a tempered water bath (ministat 125, Peter Huber Kältemaschinenbau GmbH, Offenburg, DE). A constant temperature of 25 ± 0.1 °C is automatically maintained based on temperature readings measured close to the membrane surface using a needle probe.

TMP is detected by measuring the pressure inside the filtration cell relative to the surrounding atmospheric pressure using a precision pressure gauge (P-10, WIKA SE & Co. KG, Klingenberg, DE).

Constant flux is automatically maintained by using a PID-controlled micro gear pump (mzr-7205, HNP Mikrosysteme GmbH, Schwerin, DE) coupled online to a highly precise coriolis mass-flow meter (mini Cori-Flow M13, Bronkhorst High-Tech B.V., Ruurlo, NL). The constant flux condition is additionally controlled by time-resolved recording of the produced permeate mass by using a balance (EW 3000-2M, KERN & SOHN GmbH, Balingen-Frommern, DE). The (optionally) stirred feed tanks shown in Figure 2 contain particle-free water sources of different ionic strengths. Both tanks are hydrostatically decoupled and allow the change of feed water source while the filtration is in progress. A defined foulant mass can be transferred into the filtration cell by injecting a stable particle dispersion with a known particulate or colloidal content into the feed water stream. The dosing point is located directly upstream of the gear pump.

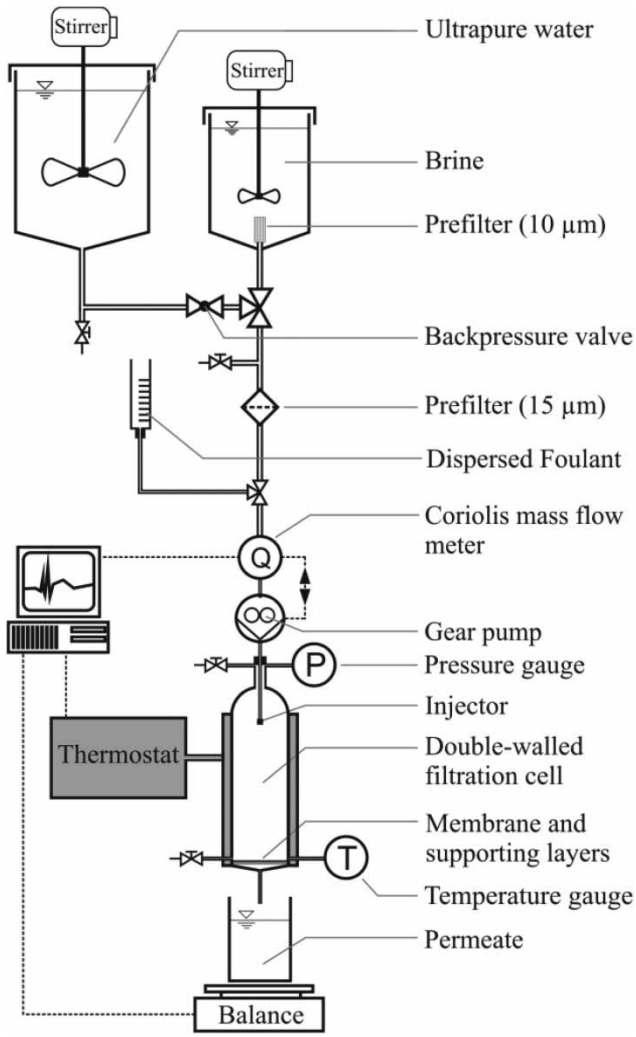

Figure 2 | Schematic drawing of the experimental plant.

Membranes

All DE filtration experiments were performed using DOW FILMTEC™ NF270 membranes. NF270 is a thin film composite poly(piperazine-amide) NF membrane known to have a NaCl retention of below 60% (Tang *et al.* 2007; Wang *et al.* 2014) and a molecular weight cut-off of roughly 270 g/mol (Rodrigues *et al.* 2010). In our own measurements the pure water hydraulic resistance of NF270 (at 50 $lm^{-2}h^{-1}$) was experimentally determined to be $2.43(\pm0.07)\cdot10^{13}$ m^{-1}. Surface zeta potential was determined to be −46.2(±1.9) mV using Zetasizer Nano ZS with a measuring cell ZEN1020 (Malvern Instruments Ltd, Malvern, UK). For each experiment a new membrane was used, which was thoroughly

rinsed with water and kept soaking in ultrapure water for a minimum of 12 h before usage.

Feed waters

Particle- and salt-free water (PW) was generated from tap-water by applying mixed bed ion exchange (TKA DI 2800, Thermo Scientific, Waltham, MA, USA) followed by an in-line particle filter with a (temporal) change in the feed water quality, pore size of 0.2 μm (AcroPak 500, Pall Corporation, Port Washington, NY, USA). The produced water meets the requirements of ultrapure water (quality class 1) according to German norm DIN ISO 3696. Consistent water quality was guaranteed by performing frequent quality checks. Saline feed water (SW) with constant ionic strength was produced by dissolving 4 g/l NaCl (≥99.5%, p.a., Carl Roth GmbH + Co. KG, Karlsruhe, DE) in ultrapure water.

Model foulants

In order to maintain well-defined filtration conditions, all fouling experiments were performed using monodisperse polystyrene (PS) particle standards (Bangs Laboratories Inc., Fishers, IN, USA). For both applied standards additional particle-size and zeta-potential measurements were performed by using Zetasizer Nano ZS (Malvern Instruments Ltd, Malvern, UK). Results and further specifications are given in Table 1. All measurements were performed in dispersion with ultrapure water. The respective dispersion was stable for at least 24 h. No significant effect on dispersion stability was observed when up to 10 g/l NaCl was added to the dispersion.

Table 1 | Specifications of the applied particle-size standards

Property	PS 28	PS 280
Particle size (according to manufacturer)	28 nm	280 nm
Particle size (own measurement)	27.56 (±0.98) nm	291.85 (± 2.82) nm
Polydispersity index	0.08 (±0.01)	0.01 (±0.01)
Size distribution	Monodisperse	Monodisperse
Particle shape	Spherical	Spherical
Material density	1.05 g/cm^3	1.05 g/cm^3
Zeta-potential	−45.76 (±2.65) mV	−48.52 (±1.02) mV

Experimental procedure

All fouling experiments depicted in the present study were performed by following a strict experimental procedure. According to this procedure each experiment was subdivided into a variable number of individual filtration phases. Each phase started with a specific change in the applied filtration conditions and ended with the establishment of an associated steady-state *TMP* maintained for at least 1 h.

This procedure allowed, by selectively adding or detracting an individual resistance contributor to or from the system, the change in steady-state TMP' to be directly related to the corresponding steady-state hydraulic resistance R' of that contributor. In the present case the three major resistances are the resistance of the membrane (R_M) the CP-layer (R_{CP}), and the fouling layer (R_F). By considering the resistances as connected in series, Darcy's law can be applied to calculate the individual hydraulic resistances from their relative contributions to the overall pressure loss at steady-state TMP'_{tot} as

$$R'_{tot} = R'_M + R'_{CP} + R'_F = \frac{TMP'_{tot}}{\eta_w \dot{J}_M} = \frac{\Delta p'_M + \Delta \pi'_M + \Delta p'_F}{\eta_w \dot{J}_M} \quad (1)$$

In this relation the index $'$ indicates that the corresponding parameter is measured under steady-state conditions (after a steady state in TMP has been reached); η_w represents the dynamic viscosity of pure water.

Since for each fouling experiment a new membrane was applied, each experiment started with determining the pressure loss across the membrane $\Delta p'_M$ by filtering ultrapure water at a constant rate of 50 lm^{-2}h^{-1}. In the subsequent phases the osmotic pressure loss $\Delta \pi'_M$ and the pressure loss across a fouling layer $\Delta p'_F$ were individually determined by measuring the increase in TMP'_{tot} associated with a respective (temporal) change in the feed water quality. In the case of $\Delta p'_F$ the feed water was temporarily spiked with foulant particles that settled onto the membrane surface. The temporal filtration of a salt solution was found to have no permanent effect on

the pure water hydraulic resistance of the applied NF270 membranes.

Normalization of R'_F with respect to the filtered foulant mass M_F per membrane area A_M gives the specific hydraulic resistance at steady state α'_F

$$\alpha'_F = \frac{R'_F A_M}{M_F} = \frac{R'_F}{\tilde{M}_M} \quad (2)$$

in which $\tilde{M}_M$ is the surface loading of the membrane or 'membrane load'.

RESULTS AND DISCUSSION

Effect of membrane load in a salt-free environment

Figure 3 shows the development of the hydraulic resistance of a discontinuously built colloidal fouling layer. The layer is formed in three distinct steps by filtering equivalent amounts of 28 nm PS beads in a salt-free environment at a constant flux of 50 $lm^{-2}h^{-1}$. Between the individual filtration steps constant flux was maintained by filtering PW until a steady state in hydraulic resistance was achieved. Figure 3 shows a strictly linear relationship between particle load and hydraulic resistance, which is a basic requirement for the application of model relations based on Darcy's law. However, the declining progression of the specific hydraulic resistance plotted on the right vertical axis shows that the relation cannot be considered linear over the complete range of particle loadings. This finding is most possibly due to the well-known effect that the particle layers that are immediately adjacent to the membrane surface usually create a significantly higher hydraulic resistance than the more distant layers (Yim & Kim 2000; Park *et al.* 2008; Mendret *et al.* 2009; Taheri *et al.* 2013). This fact implies that Darcy-type relations are generally not valid in the lower range of membrane loadings.

According to DLVO theory, electrostatic repulsion forces acting between like-charged particles are considered to have the longest range in low ionic strength dispersions, causing an insuperable energy barrier and thus the dispersion to be stable. Hence in PW experiments agglomeration effects between the used PS particles with strongly negative surface potential (cf. Table 1) are rather unlikely to occur outside the fouling layer. Studies performed by Nirschl *et al.* showed that the filtration of stable colloidal dispersions led to the formation of compact layers with low porosity and homogenous pore-size distribution (Nirschl & Schäfer 2005).

However because of strong hydrodynamic forces the energy barrier is overcome in the fouling layer, causing high compactness. This basic assumption can be theoretically supported by applying fundamental electrostatic concepts. According to Israelachvili (2011) the electrostatic

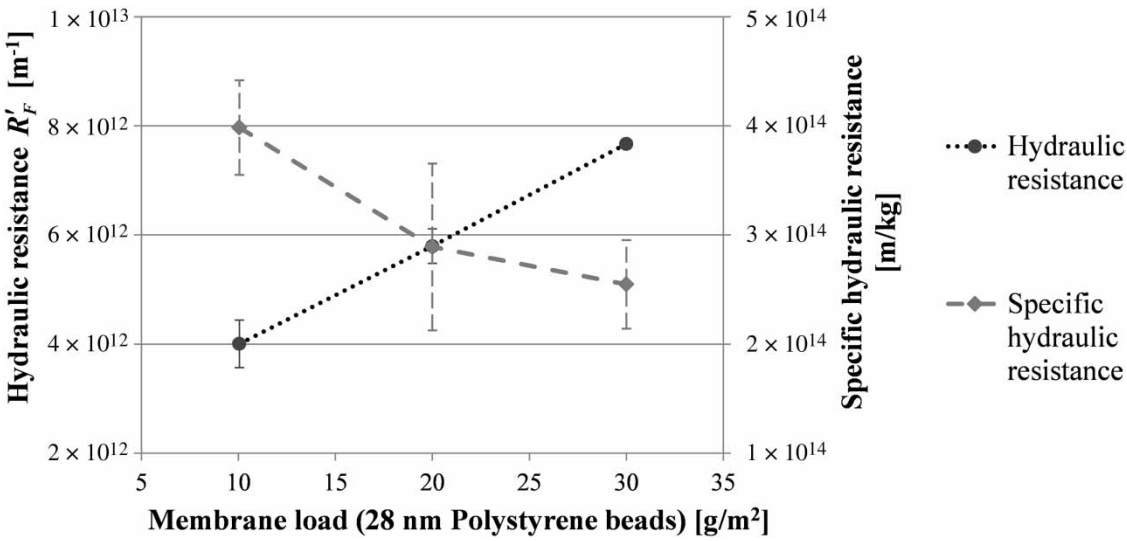

Figure 3 | Dependence of fouling layer resistance on membrane load with 28 nm polystyrene beads.

repulsion force acting between two spherical particles 1 and 2 can be estimated by using the following equation:

$$F_{el} = \frac{d_{eff}}{\lambda_D} 32\pi \varepsilon_0 \varepsilon_r \left(\frac{k_B T}{e}\right)^2 \tanh\left(\frac{z_i e \psi_1}{4 k_B T}\right) \cdot \tanh\left(\frac{z_i e \psi_2}{4 k_B T}\right) \times \exp^{-\frac{h}{\lambda_D}} \quad (3)$$

in which d_{eff} is the effective particle diameter with

$$d_{eff} = \frac{d_{p1} \cdot d_{p2}}{d_{p1} + d_{p2}} \quad (4)$$

By using the parameter values specified in Table 2, Equation (3) yields $1.9 \cdot 10^{-13}$ N for the maximum repulsing force (attractive forces are disregarded). This force is counteracted by the combined structural and frictional force F_{fr} imposed on a single particle.

Considering a monodisperse colloidal layer as consisting of an unknown number of particle sublayers, each containing an equivalent number of particles that are exposed to identical structural and frictional forces F_{fr}, and further assuming that the pressure drop, as presumed by Darcy's law, linearly increases sublayer by sublayer with layer depth, then F_{fr} is a function of the ratio of layer thickness at point z (ℓ_z) to the total layer thickness (ℓ_F) and the inflow cross-section of a representative particle A_p:

$$F_{fr} = \Delta p'_F \cdot \frac{\ell_z}{\ell_F} \cdot A_p \quad (5)$$

With respect to the measured data shown in Figure 3, $\Delta p'_F$ for a relatively thin 28 nm PS layer (membrane load 10 g/m^2) is ~23,000 Pa. Equating Equations (3) and (5) and solving yields 0.14 for ℓ_z/ℓ_F. This result indicates that, even for rather thin fouling layers, only in less than 1% of all constituting sublayers (monolayers) repulsive forces are not overcome by frictional forces.

In this simple estimation the pressure loss is assumed to be a linear function of the layer depth. This assumption is, to some extent, unrealistic since, due to the influence of neighboring particles, densely packed particle layers produce higher hydraulic resistances (and therefore pressure loss) than electrostatically stabilized monolayers with comparably high porosities. Nevertheless, the consideration of this instance as well as the incorporation of the effect of attractive van der Waals forces in this context yields only a slightly higher value of 5.5% (Keller 2016).

By taking into account these considerations it can be accepted that monodisperse layers that are built up (and consolidated until reaching a steady state) in PW feature porosities close to 36%, which corresponds to the densest random packing of equal spheres (Gotoh & Finney 1974).

If, however, a layer porosity of 36% is applied in calculations with the traditional models of Kozeny–Carman (KC), using $\kappa = 5$ as the porosity-dependent constant, Rumpf, Happel, and Kuwabara (see the Introduction), these models strongly overestimate the respectively measured resistance, as depicted in Figure 4.

Table 2 | Parameters to be used with Equation (3)

Parameter	Value
ψ_1; $\psi_2 (=\zeta_{PS(28nm)})$	−45.76 mV
λ_D	960 nm
d_{eff}	14 nm
z_i	1
ϵ_r (25 °C)	78.3
T	298.15 K
h	0.4 nm

Effect of colloid size and particle size distribution in a salt-free environment

In Figure 5 the measured specific resistances of different colloid size (28 nm; 280 nm; mixture of both) PS fouling layers are compared to the respective KC-predictions. Since smaller-size particles (diameter d_d) fill-up spaces between the larger-size particles (diameter d_D), a bi-disperse particle layer is generally considered to have a lower porosity than a monodisperse layer made from identical material. To account for this effect the semi-empirical correlation of Dias *et al.* (2004) is used to calculate the porosity ε_{bi} of the bi-disperse mixture from the given volume fraction of larger-size particles in the mixture X_D:

$$\varepsilon_{bi} = \frac{\varepsilon_d^0 (1 - x_D) \exp\left(1, 2264 x_D^{1/\sqrt{d_d/d_D}}\right)}{1 - \varepsilon_d^0 x_D} \quad (6)$$

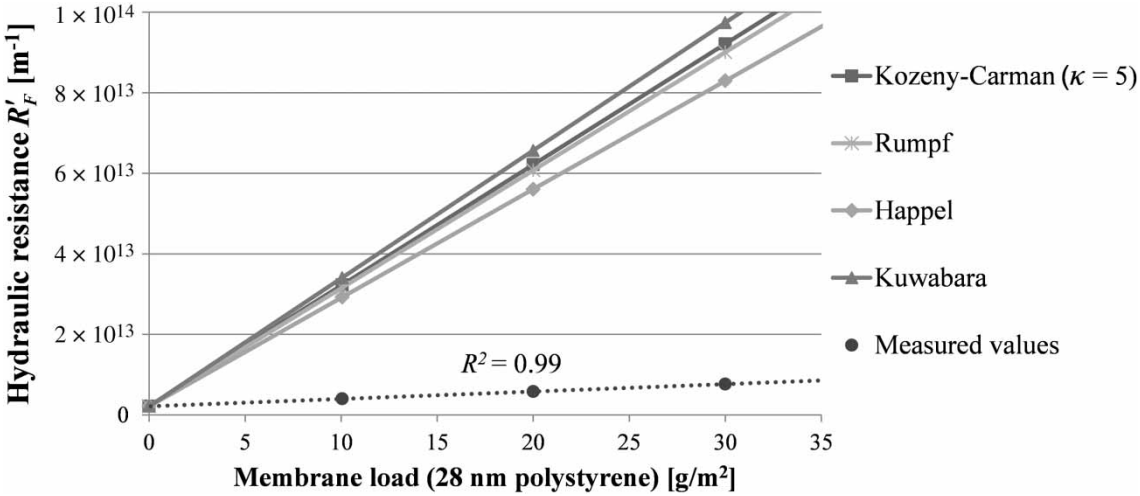

Figure 4 | Dependence of hydraulic fouling layer resistance on membrane load: comparison of measured values with predications made by established macroscale model theories. R^2 represents the coefficient of determination.

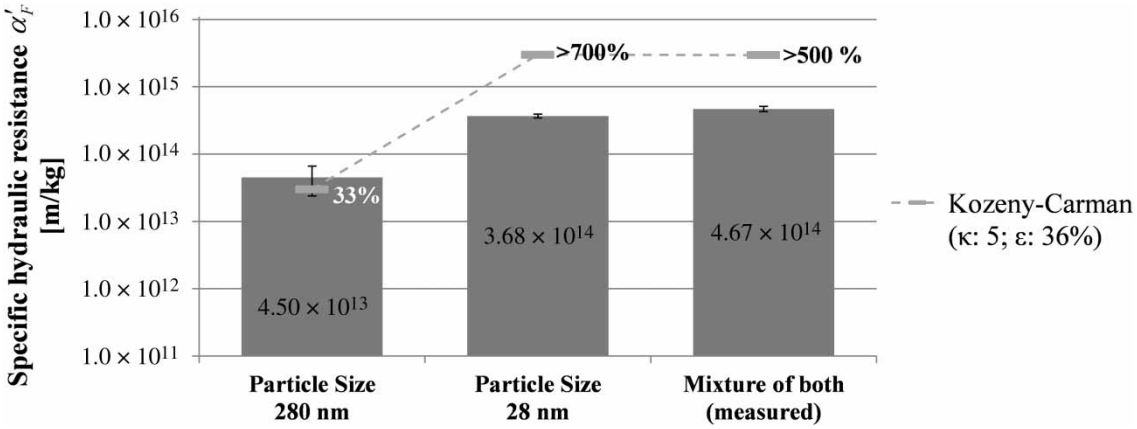

Figure 5 | Comparison of KC-predictions with measured specific hydraulic resistances for different colloid size fouling layers. Percentage values correspond to the deviation of the KC-prediction based on the respective reading.

In accordance with the prior considerations the porosity of a monodisperse layer of the smaller-size particle fraction ε_d^0 is assumed to be 36%.

The results depicted in Figure 5 show that the overestimation of layer resistance by the model theory, as described in the preceding section, only applies to layers that contain 28 nm particles. For monodisperse 280 nm particle layers, the KC-results (cf. markers labeled 'Kozeny-Carman' in Figure 5) agree with measured values within the acceptable margin of error. This result indicates that in the colloidal size range an additional strongly size-specific effect has to be considered that reduces the measured hydraulic resistance with decreasing particle size. Since both applied particle sizes are considerably bigger than the pore size of the applied nanofiltration membrane, obstruction of pores (as proposed by classical pore-blocking models) is not considered a significant reason for the measured fouling-related resistance increase. The remaining possible causes of this phenomenon are manifold. As examples an increasing deviation from the no-slip flow condition in nanoscale channels (Choi *et al.* 2003) or the formation of a heterogeneous layer structure due to the increasing relevance of surface interactions can be mentioned.

When the initially described assumption, regarding the balance of inter-particle hydrodynamic and electrostatic forces, is correct, a colloidal fouling layer in steady state should have reached a consolidated state where the strongly distance-dependent adhesive forces are fully established and the particle arrangement is mostly fixed. Thus, it is hypothesized that if a bi-disperse particle layer is formed by subsequent filtration of particle sizes (with an intermediate consolidation phase between the filtration steps) the structure of the first built layer should be at least partially maintained when the second particle layer is generated on top. It is to be expected that the resulting layer structure causes a different specific hydraulic resistance than the mixed layer shown in Figure 5. This hypothesis is confirmed by the results of the respective layer formation experiment shown in Figure 6. In the case of the layers built in a two-step procedure (280 on 28 nm; 28 on 280 nm) the second particle size was filtered after the initially produced layer had adopted a steady-state hydraulic resistance. The depicted results basically confirm the assumption of a rather strong structural integrity of once consolidated layers.

The results indicate that, when 280 nm particles are filtered on top of a consolidated layer of 28 nm particles, an almost ideal two-layer structure is formed (cf. Figure 7(a)) that is only marginally higher than the value calculated from the individually measured monodisperse layer resistances (labeled 'sum of separate measurements'). The significantly higher resistance of a layer built with an opposite particle size sequence (28 on 280 nm) is most likely due to the infiltration of 28 nm particles into the existing skeleton of larger-size particles. While passing the skeleton it is quite likely that a portion of the smaller-size particles is retained within the skeleton by some 'deep bed filtration effect' (cf. Figure 7(b)). The retained fraction does not contribute to the formation of a highly compact particle zone in the vicinity of the membrane (compaction zone). Since this compaction zone is assumed to be the major source of resistance in the bi-disperse layer, the deep bed filtration effect potentially reduces the hydraulic resistance of the bi-disperse layer. When particle sizes are filtered simultaneously this deep bed filtration effect is absent, which leads to the formation of the compaction zone in its maximum extent (cf. Figure 7(c)) and a maximum hydraulic resistance respectively (cf. Figure 6). A rather perfect accumulation of all 28 nm particles in the compaction zone was confirmed by scanning electron microscopy (results provided elsewhere (Keller 2016)).

Effect of ionic strength

It has been shown in numerous studies that the colloidal fouling layer resistance is strongly affected by the feed ionic strength. The possible reasons for that affection are manifold and will not be discussed in detail at this point.

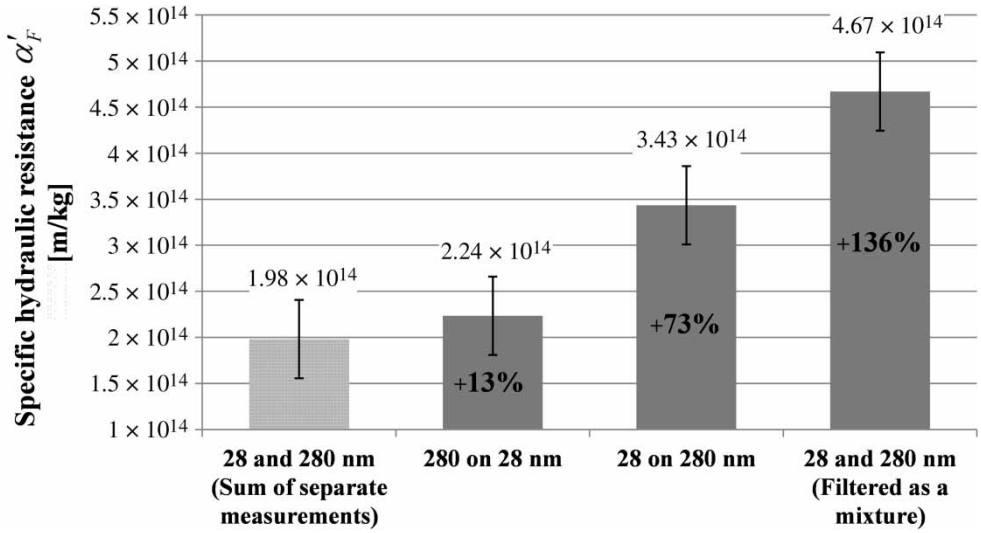

Figure 6 | Specific hydraulic resistance of bi-disperse layers built by different particle-size filtration sequences. Total membrane load is identical in each depicted case.

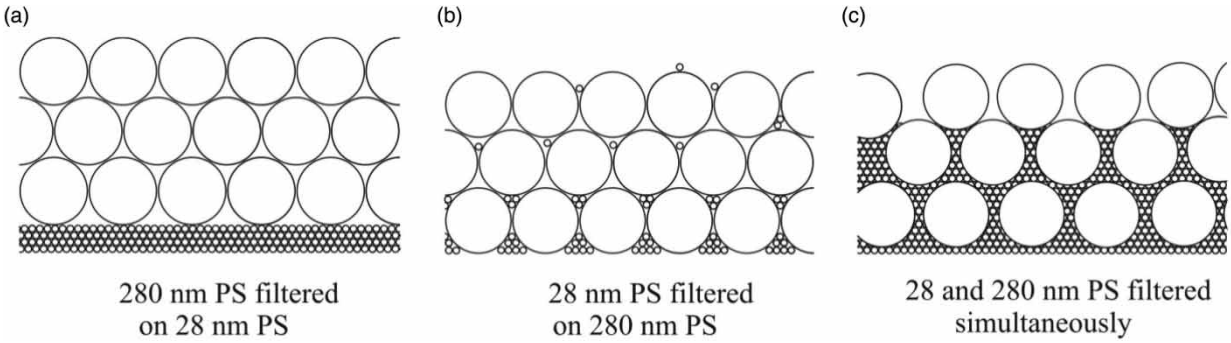

Figure 7 | Schematic representation of different bi-disperse PS-layer structures.

Generally there has to be distinction between dispersion destabilizing effects, which are basically due to shielding of repulsive electrostatic interaction-forces, and the effects which occur after a fouling layer is formed (i.e. CEOP). While destabilizing effects are considered to (irreversibly) influence the fouling layer structure (mainly during its formation), all other effects are related to interactions between an established fouling layer structure and the ion distribution and movement within it.

In the present case the experimental setup allows the differentiation of both influences. With respect to the results shown in the preceding section, it is thereby assumed that a colloidal layer that was fully consolidated in PW is only to a minor extent affected by destabilizing effects. Changes in hydraulic layer resistance measured in association with a change in feed ionic strength can therefore be mainly related to the second group of influences. In contrast, layers that are formed in a salt-containing feed (SS) are affected by a combination of both influences.

The three bars on the left side of Figure 8 show hydraulic resistances of monodisperse PS (28 nm) layers that were formed in either PW or SS. An important advantage of the applied experimental setup is that the feed water source can be arbitrarily changed after a fouling layer has been established. The second and third bars (from the left), therefore, show the resistance of layers where the resistance measurement was performed while filtering feed water with an ionic strength different to that applied during fouling-layer formation. Results clearly indicate that the ionic strength has a definite effect on hydraulic resistance. It further indicates that the hydraulic resistance of a fouling layer is significantly more affected when its consolidation has been performed in SS. Since electrostatic repulsion forces are shielded by dissolved ions, the range of

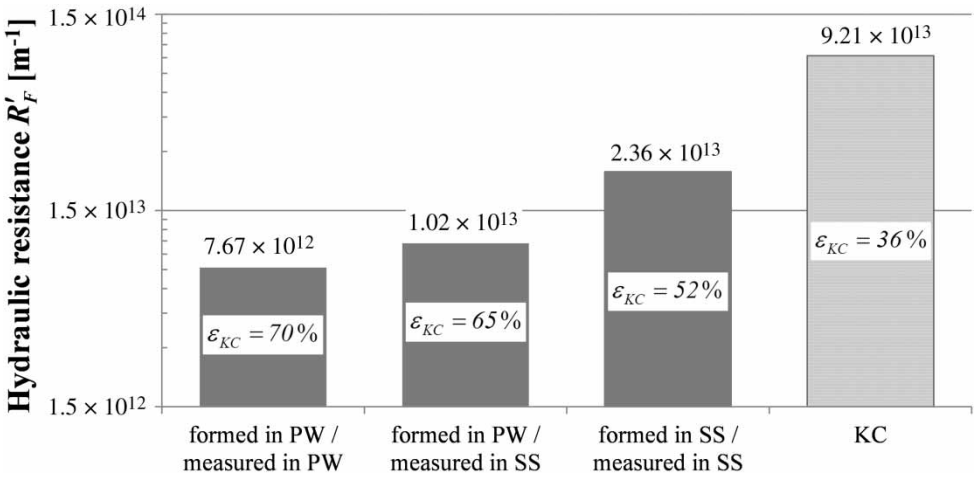

Figure 8 | Layer porosities as predicted by the Kozeny–Carman equation. Total membrane load in each depicted case is 30 g PS-28 nm per m^2.

electrostatic forces is supposed to be biggest in PW (Israelachvili 2011). When the identified ionic strength dependency of hydraulic layer resistance is solely attributed to the changing inter-particle distances maintained by electrostatic repulsion forces, the porosity of a layer formed in SS (low inter-particle distance) should be significantly lower than that of a layer formed in PW (high inter-particle distance). In order to prove this assumption, the theoretical layer porosities were calculated for each measured resistance value by using the KC-relation ($\kappa = 5$). For easier classification of the results the resistance for a hypothetical layer of particles with direct surface contact between the particles ($\varepsilon = 36\%$) is shown on the right.

The respective values given in Figure 8 show that even for layers formed in SS, a porosity of more than 50% has to be accepted in order to match predictions with measured values. With respect to the previously provided considerations, such high values appear to be rather unrealistic. A permanent increase in inter-particle spacing due to electrostatic repulsion effects, therefore, seems to be a rather unlikely explanation for the high discrepancy between measured values and model predictions.

Figure 9 shows the development of hydraulic resistances with increasing membrane load for two layers that are established by filtering different ionic strength colloidal dispersions. Independent of the feed ionic strength both graphs show a strict linear relation between resistance increase and membrane load. Therefore, in order to describe the layer resistance, Darcy-type relations seem to be applicable when the influence in feed ionic strength is respectively considered.

The respectively measured values are shown in Figure 9. The results demonstrate that most of the difference in resistance that is associated with the different ionic strengths applied during layer formation cannot be undone by future changes of the feed ionic strength. It is further noteworthy that the magnitude of the minor reversible share of the ionic strength dependent difference in hydraulic layer resistance is nearly identical regardless of whether the ionic strength is increased or decreased. It can therefore be assumed that both processes have the same cause.

Electro-osmotic effects, however, are not considered a probable cause, since relevant sources (Michaels & Lin 1955; Abaza 1966) clearly show that their resistance-increasing effect is more significant when the electrical conductivity (or ionic strength) of the fluid is low. In the current case a reversed dependency is detected.

CONCLUSIONS

Within the presented study a measuring approach is proposed and tested that enables the determination of hydraulic resistances generated by any kind of spatially homogeneous layer that covers the feed site membrane surface. The method particularly distinguished itself from

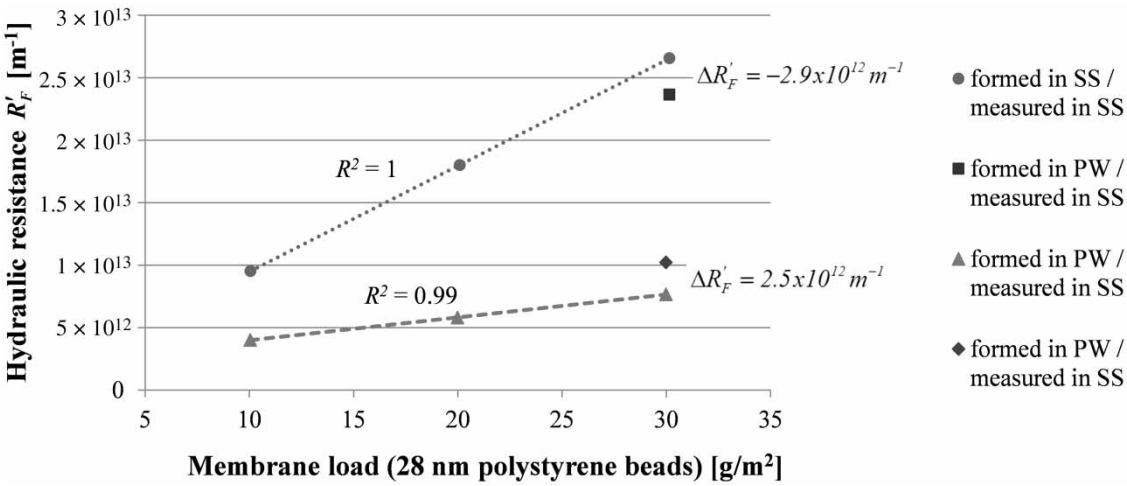

Figure 9 | Reversibility of the ionic strength dependent share of the steady-state hydraulic layer resistance (for PS-28 nm). R^2 represents the coefficient of determination.

existing concepts by the fact that measured resistances, contributed by any (steady-state) solid or gel-like fouling layer, can be clearly separated from resistances contributed by a diffuse (CP-)layer with undefined phase boundaries, even if the two layer types occur simultaneously and superpose each other. By an adequate usage of that feature it is also possible to quantify the relevance of coupling mechanisms between the two resistance types. The introduced method was successfully tested by performing filtration experiments using idealized model foulants with known physicochemical properties. Besides its general applicability in fundamental research a potential application for the highly standardized and reproducible approach is the development of new indexing procedures (e.g. indicating fouling propensities of different membrane materials or feed waters). These to-be-developed methods would possess the advantage of considering the effect of the CP-dependency of the fouling layer resistance, which is commonly ignored by most existing concepts.

ACKNOWLEDGEMENTS

The authors gratefully acknowledge funding by the German Research Foundation (DFG).

REFERENCES

Abaza, M. M. I. 1966 *Streaming Current and Streaming Potential Induced by Water Flow Through Porous Media*. PhD Thesis, Department of Civil Engineering, Utah State University, Utah, USA.

Choi, C. H., Westin, K. J. A. & Breuer, K. S. 2003 Apparent slip flows in hydrophilic and hydrophobic microchannels. *Physics of Fluids* **15** (10), 2897–2902.

Dias, R. P., Teixeira, J. A., Mota, M. G. & Yelshin, A. I. 2004 Particulate binary mixtures: dependence of packing porosity on particle size ratio. *Industrial and Engineering Chemistry Research* **43** (24), 7912–7919.

Dullien, F. A. L. 1992 *Porous Media: Fluid Transport and Pore Structure,* 2nd edn. Academic Press, Inc., San Diego, CA, ch. 3, pp. 237–317.

Gotoh, K. & Finney, J. L. 1974 Statistical geometrical approach to random packing density of equal spheres. *Nature* **252** (5480), 202–205.

Hoek, E. M. V. & Elimelech, M. 2003 Cake-enhanced concentration polarization: a new fouling mechanism for salt-rejecting membranes. *Environmental Science & Technology* **37** (24), 5581–5588.

Israelachvili, J. N. 2011 *Intermolecular and Surface Forces,* 3rd edn. Academic Press, Waltham, MA, USA, ch. 14, pp. 291–340.

Keller, M. 2016 Zur Bedeutung hydraulisch bedingter Deckschichtwiderstände beim Fouling salzrückhaltender Membranen unter besonderer Berücksichtigung von Kopplungseffekten. Dissertation, Fakultät für Ingenieurwissenschaften, Abteilung Maschinenbau, Universitaet Duisburg-Essen, Duisburg, Germany.

Kim, S., Lee, S., Lee, E., Sarper, S., Kim, C. H. & Cho, J. 2009 Enhanced or reduced concentration polarization by membrane fouling in seawater reverse osmosis (SWRO) processes. *Desalination* **247** (1–3), 162–168.

Lipp, P., Gimbel, R. & Frimmel, F. H. 1994 Parameters influencing the rejection properties of FT30 membranes. *Journal of Membrane Science* **95** (2), 185–197.

Mahlangu, T. O., Hoek, E. M. V., Mamba, B. B. & Verliefde, A. R. D. 2014 Influence of organic, colloidal and combined fouling on NF rejection of NaCl and carbamazepine: role of solute–foulant–membrane interactions and cake-enhanced concentration polarisation. *Journal of Membrane Science* **471**, 35–46.

Masliyah, J. H. & Bhattacharjee, S. 2006 *Electrokinetic and Colloid Transport Phenomena,* John Wiley & Sons, Inc., Hoboken, NJ, USA, ch. 9.4.1, pp. 328–333.

Mendret, J., Guigui, C., Schmitz, P. & Cabassud, C. 2009 In situ dynamic characterisation of fouling under different pressure conditions during dead-end filtration: compressibility properties of particle cakes. *Journal of Membrane Science* **333** (1–2), 20–29.

Michaels, A. S. & Lin, C. S. 1955 Effects of counterelectro-osmosis and sodium ion exchange on permeability of kaolinite. *Industrial & Engineering Chemistry* **47** (6), 1249–1253.

Nirschl, H. & Schäfer, B. 2005 Distinction between electrostatic and electroviscous effects on the permeability of colloidal packed beds. *Chemical Engineering and Technology* **28** (8), 862–866.

Park, C., Lee, Y. H., Lee, S. & Hong, S. 2008 Effect of cake layer structure on colloidal fouling in reverse osmosis membranes. *Desalination* **220** (1–3), 335–344.

Rodrigues, C., Cavaco Morão, A. I., de Pinho, M. N. & Geraldes, V. 2010 On the prediction of permeate flux for nanofiltration of concentrated aqueous solutions with thin-film composite polyamide membranes. *Journal of Membrane Science* **346** (1), 1–7.

Shen, L. & Chen, Z. 2007 Critical review of the impact of tortuosity on diffusion. *Chemical Engineering Science* **62** (14), 3748–3755.

Sim, L. N., Ye, Y., Chen, V. & Fane, A. G. 2011 Investigations of the coupled effect of cake-enhanced osmotic pressure and

colloidal fouling in RO using crossflow sampler-modified fouling index ultrafiltration. *Desalination* **273** (1), 184–196.

Sim, S. T. V., Taheri, A. H., Chong, T. H., Krantz, W. B. & Fane, A. G. 2014 Colloidal metastability and membrane fouling – effects of crossflow velocity, flux, salinity and colloid concentration. *Journal of Membrane Science* **469**, 174–187.

Taheri, A. H., Sim, L. N., Haur, C. T., Akhondi, E. & Fane, A. G. 2013 The fouling potential of colloidal silica and humic acid and their mixtures. *Journal of Membrane Science* **433**, 112–120.

Tang, C. Y., Kwon, Y. N. & Leckie, J. O. 2007 Fouling of reverse osmosis and nanofiltration membranes by humic acid – effects of solution composition and hydrodynamic conditions. *Journal of Membrane Science* **290** (1–2), 86–94.

Tang, C. Y., Chong, T. H. & Fane, A. G. 2011 Colloidal interactions and fouling of NF and RO membranes: a review. *Advances in Colloid and Interface Science* **164** (1–2), 126–143.

Wang, J., Mo, Y., Mahendra, S. & Hoek, E. M. V. 2014 Effects of water chemistry on structure and performance of polyamide composite membranes. *Journal of Membrane Science* **452**, 415–425.

Yim, S. S. & Kim, J. H. 2000 An experimental and theoretical study on the initial period of cake filtration. *Korean Journal of Chemical Engineering* **17** (4), 393–400.

First received 3 August 2016; accepted in revised form 26 October 2016. Available online 14 December 2016